Published in final edited form as:
J Pharm Sci. 2014 November ; 103(11): 3782–3792. doi:10.1002/jps.24131.

Design and Evaluation of a Novel Trifluorinated Imaging Agent for Assessment of Bile Acid Transport Using Fluorine Magnetic Resonance Imaging

Diana Vivian[1], **Kunrong Cheng**[2], **Sandeep Khurana**[2], **Su Xu**[3], **Paul A. Dawson**[4], **Jean-Pierre Raufman**[2], and **James E. Polli**[1]

[1]Department of Pharmaceutical Sciences, University of Maryland School of Pharmacy, Baltimore, Maryland 21230

[2]Department of Medicine, University of Maryland School of Medicine, Baltimore, Maryland 21230

[3]Department of Diagnostic Radiology and Nuclear Medicine, University of Maryland School of Medicine, Baltimore, Maryland 21230

[4]Division of Pediatric Gastroenterology, Hepatology, and Nutrition, Emory University School of Medicine, Atlanta, Georgia 30322

Abstract

Previously, we developed a trifluorinated bile acid, CA-lys-TFA, with the objective of noninvasively assessing bile acid transport *in vivo* using ^{19}F magnetic resonance imaging (MRI). CA-lys-TFA was successfully imaged in the mouse gallbladder, but was susceptible to deconjugation *in vitro* by choloylglycine hydrolase (CGH), a bacterial bile acid deconjugating enzyme found in the terminal ileum and colon. The objective of the present study was to develop a novel trifluorinated bile acid resistant to deconjugation by CGH. CA-sar-TFMA was designed, synthesized, and tested for *in vitro* transport properties, stability, imaging properties, and its ability to differentially accumulate in the gallbladders of normal mice, compared with mice with known impaired bile acid transport (deficient in the apical sodium-dependent bile acid transporter, ASBT). CA-sar-TFMA was a potent inhibitor and substrate of ASBT and the Na^+/taurocholate cotransporting polypeptide. Stability was favorable in all conditions tested, including the presence of CGH. CA-sar-TFMA was successfully imaged and accumulated at 16.1-fold higher concentrations in gallbladders from wild-type mice compared with those from Asbt-deficient mice. Our results support the potential of using MRI with CA-sar-TFMA as a noninvasive method to assess bile acid transport *in vivo*.

Correspondence to: Jean-Pierre Raufman (Telephone: +410-328-8728; Fax: +410-328-8315; jraufman@medicine.umaryland.edu); James E. Polli (Telephone: +410-706-8292; Fax +410-706-5017; jpolli@rx.umaryland.edu).

This article contains supplementary material available from the authors upon request or via the Internet at http://onlinelibrary.wiley.com/.

Keywords

fluorine MRI; bile acid malabsorption; enterohepatic circulation; imaging methods; intestinal absorption; site-specific delivery; transporters; targeted drug delivery; bile acid transporters; biliary excretion

Introduction

Bile acid homeostasis is maintained by balancing hepatic synthesis with an efficient enterohepatic recirculation, and the major biosynthetic enzymes and transporters have been identified. After their synthesis from cholesterol in the liver, bile acids are conjugated to glycine or taurine, and secreted into bile by the bile salt export pump (BSEP; *ABCB11*) and to a lesser extent by the multidrug resistance-associated protein 2 (MRP2; *ABCC2*). Between meals, bile is stored in the gallbladder. In response to a meal, the gallbladder contracts and bile acids are emptied into the duodenum where they increase lipid solubility through micelle formation. Bile acids are passively absorbed throughout the small intestine, as well as actively absorbed by enterocytes in the terminal ileum via the apical sodium-dependent bile acid transporter (ASBT, *SLC10A2*). After uptake by enterocytes, bile acids are effluxed into the portal circulation by the organic solute transporters (OSTα-OSTβ; *SLC51A*, *SLC51B*) and to a lesser extent by multidrug resistance protein 3 (MRP3; *ABCC3*). At the liver, the bile acids are taken up by hepatocytes via the Na^+/taurocholate cotransporting polypeptide (NTCP, *SLC10A1*) and the organic anion transporting polypeptides (OATPs) for resecretion into bile. This enterohepatic circulation of bile acids maintains the human bile acid pool between 2 and 4 g. Bile acids circulate several times daily with less than 10% lost in feces.[1,2]

Bile acid malabsorption (BAM), characterized by excess fecal bile acids and chronic watery diarrhea, is often misdiagnosed as diarrhea-predominant irritable bowel syndrome (IBS-D).[3] BAM is considered responsible for 30%–50% of unexplained chronic diarrhea.[4–7] Although BAM can be attributed to ileal resection/damage or rare ASBT mutations, the cause of most cases of idiopathic BAM is unknown. Recent advances in understanding this disease suggest that overproduction of bile acids resulting from deficient fibroblast growth factor (FGF)-19 may be a common feature of BAM.[8] FGF19 is part of the mechanism for feedback inhibition of hepatic bile acid synthesis from cholesterol, and regulation of bile acid synthesis is impaired in its absence. This dysregulation leads to hepatic overproduction of bile acids, exceeding the ileal absorptive capacity, thereby increasing colonic exposure and diarrhea.

In the United States, diagnosis of BAM is limited by the lack of sensitive, specific, and cost-effective tests. ^{75}Se-homocholic acid-taurine (HCAT), a ^{75}Se-labeled gamma-emitting synthetic bile acid used to measure intestinal uptake of bile acids, is available for use in selected European countries, but has not been approved by the United States Food and Drug Administration (US FDA).[9] Diagnostic criteria for this test are based on the percentage of ^{75}Se-HCAT retained in the body 1 week after oral administration. Other methods to diagnose BAM include ^{14}C-taurocholate stool measurement,[10] 7α-hydroxy-4-cholesten-3-one serum measurement as a biomarker of bile acid formation,[11] and blood FGF19

measurement[12] (inversely related to 7α-hydroxy-4-cholesten-3-one levels). However, these methods are time consuming, difficult, not readily available, or not validated clinically. Hence, BAM is often diagnosed by administering bile acid sequestrants, such as colesevelam, in a therapeutic trial,[13,14] an approach that is not US FDA approved for this indication, lacks specificity, and has a high rate of false-negative diagnosis.[7]

To address these limitations, we previously proposed to develop a novel approach to diagnosing BAM by using *in vivo* imaging of a fluorinated bile acid analogue with ^{19}F magnetic resonance imaging (MRI).[15] We hypothesized that tracking a tagged bile acid molecule by imaging its accumulation in the gallbladder would allow differentiation between normal and impaired bile acid transport. ^{19}F MRI was chosen because it is noninvasive and involves no ionizing radiation. ^{19}F, the naturally occurring, stable (i.e., nonradioactive) isotope of fluorine, is second to only ^{1}H MRI in terms of MRI sensitivity. Unlike ^{1}H MRI, with ^{19}F MRI there is no endogenous background signal,[16] thereby providing the potential for improved signal-to-noise-ratio. ^{19}F MRI signal intensity increases proportionally to fluorine concentration, so tracer amounts can be compared and quantified.[17]

CA-lys-TFA, a conjugate of trifluoroacetyl-lysine and cholic acid, was previously synthesized and tested *in vitro* for stability and ASBT and NTCP transport affinity.[15] After a preliminary pharmacokinetic profile was obtained in mice, CA-lys-TFA was orally dosed and imaged *in vivo* in the mouse gallbladder by ^{19}F MRI.[18] CA-lys-TFA accumulated in significantly larger amounts in wild type (WT) mouse gallbladders compared with gallbladders of Asbt-deficient (*Slc10a2*$^{-/-}$) mice, which have severely impaired bile acid absorption, a reduced bile acid pool, and higher levels of fecal bile acids.[19] The gallbladders of Asbt-deficient mice showed no fluorine signal when imaged using ^{19}F MRI, whereas those of WT mice showed robust ^{19}F signals. Overall, these studies showed that ^{19}F MRI of a fluorinated bile acid probe is a feasible means to identify impaired bile acid transport *in vivo*.

An important limitation of CA-lys-TFA as an imaging agent is its susceptibility to bacterial metabolism. Like native bile acids, Ca-lys-TFA is susceptible to removal of its amino acid side chain by choloylglycine hydrolase (CGH), a bacterial bile acid deconjugating enzyme located predominantly in the colon and in smaller amounts in the terminal ileum.[15] Here, our objective was to synthesize and test a fluorinated bile acid resistant to bacterial deconjugation. We believe this attribute will diminish the potential for differences in intestinal microbiota to alter probe concentrations in the enterohepatic circulation and also increase the half-life of the fluorinated bile acid probe. We report the synthesis of the novel trifluorinated bile acid CA-sar-TFMA, and its *in vitro* stability and affinity for both ASBT and NTCP. A pilot *in vivo* disposition study in mice confirmed that CA-sar-TFMA can be imaged in the gallbladder using ^{19}F MRI. Additionally, using Asbt-deficient mice as a test model, we show that oral administration of CA-sar-TFMA has potential as a novel method to diagnose impaired intestinal bile acid uptake. Collectively, our results support the suitability of CA-sar-TFMA as a ^{19}F MRI tracer to diagnose BAM.

Experimental

Materials

Taurocholate, cholic acid, trifluoroacetic anhydride, rat liver S9 fraction, trifluoroacetic acid (TFA), rat plasma, and CGH from *Clostridium perfringens* were obtained from Sigma–Aldrich (St. Louis, Missouri). N-boc-ethylene diamine was purchased from Oakwood Chemical (West Columbia, South Carolina). [^{3}H]-taurocholate (10 μ Ci/mM) was purchased from American Radiolabeled Chemicals, Inc. (St. Louis, Missouri). Trypsin, geneticin, fetal bovine serum (FBS) and Dulbecco's modified Eagle medium (DMEM) were purchased from Invitrogen (Rockville, Maryland). All other reagents and chemicals were of the highest purity available commercially.

Methods

Synthesis of CA-sar-TFMA—CA-sar-TFMA was synthesized as in Figure 1. Two milliliters (12.6 mmol) of N-boc-ethylene diamine was stirred for 15 min with 2 eq. (25.2 mmol) sodium hydroxide (NaOH) in dimethyl formamide (DMF). To this mixture, 0.6 eq. (7.6 mmol) benzyl bromoacetate was added and stirred overnight at room temperature. DMF was diluted with ethyl acetate and washed three times with 30 mL water. The product was dried with sodium sulfate and ethyl acetate was removed by vacuum. The resulting clear oil was separated by silica gel column chromatography, using an eluent of 1:1 ethyl acetate:hexane. The resulting product (Fig. 1, compound 1) showed an appropriate mass spectrometry (MS) peak of [M+1] 309.1.

Compound 1 was stirred with 1:1 dichloromethane (DCM):TFA for 15 min to remove the N-boc protecting group. Excess solvent was evaporated, yielding compound 2. Next, the compound was stirred in DCM at 0°C and 0.6 eq. (3.5 mmol) triflouroacetic anhydride was added. The mixture was allowed to return to room temperature and was stirred overnight. DCM was then evaporated under vacuum and the product was dissolved in ethyl acetate and washed with saturated sodium bicarbonate. The organic layer was dried with sodium sulfate and ethyl acetate was evaporated under vacuum. The resulting product was purified using flash column chromatography with a solvent of 30% hexane in ethyl acetate. MS showed [M +1] of 305.1 (Fig. 1, compound 3) and thin-layer chromatography (TLC) showed a single spot when stained with 10% (w/v) phos-phomolybdic acid in ethanol (EtOH) (R_f = 0.48; ethyl acetate).

Two grams (4.9 mmol) of cholic acid was stirred at room temperature for 15 min in DMF with 1 eq. (4.9 mmol) triethylamine (TEA) and 1 eq. (4.9 mmol) O-benztriazol-1-yloxytris-1,1,3,3 tetra methyl uranium hexaflourophosphate. 1 eq. (4.9 mmol) of hydroxybenzotriazole was added, and the mixture was stirred for 4 h, then the reaction was quenched with water and extracted with ethyl acetate. The organic layer was washed three times with water, dried with sodium sulfate, and solvent was evaporated under reduced pressure. MS of this resulting activated cholic acid OBt ester (Fig. 1, compound 4) showed a peak of [M+1] 526.4.

The activated OBt ester (3.4 mmol) was allowed to react with 1 eq. compound 3 (3.4 mmol) in DMF overnight at room temperature. The resulting product was extracted with ethyl

acetate, washed three times with water, dried with sodium sulfate, and the ethyl acetate was evaporated under vacuum. Compound 5 was purified on a silica gel column using an eluent of 7% methanol in DCM, resulting in a fluffy white solid (MS showed [M+23] 717.3 and [M−1] 693.4). TLC confirmed purity, as a single spot was seen when stained with 10% (w/v) phosphomolybdic acid in EtOH (R_f = 0.38; 10% methanol in DCM).

The final product, CA-sar-TFMA, was obtained by hydrogenating compound 5 in the presence of 10 weight percent palladium/carbon catalyst in EtOH for 4 h to remove the benzyl protecting group. Purity was confirmed by TLC, MS, HPLC, and ^{13}C nuclear magnetic resonance (NMR). Structural properties were confirmed with two-dimensional heteronuclear multiplebond correlation spectroscopy and heteronuclear single quantum coherence. NMR was performed on a Varian VNMRS 400 MHz machine (Agilent Technologies, Santa Clara, California) in deuterated dimethyl sulfoxide (DMSO) at 25°C. HPLC was performed on a Waters HPLC system comprised of a 1525 binary HPLC pump, a 717 plus autosampler, and a 486 tunable absorbance detector (Waters Corporation, Milford, Massachusetts) with a Restek column (ultra phenyl, 5 μM, 250 × 4.6 mm^2; Restek Corporation, Bellefonte, Pennsylvania). Flow rate was 1.0 mL/min and absorbance wavelength was 218 nm. Two isocratic methods were used. The first method utilized 30% acetonitrile (ACN) and 70% water with 0.1% formic acid. The second method employed a 67:33 (v/v) mixture of methanol and [20 mM ammonium formate, 0.5% formic acid, 0.2% TEA (pH 3)].[20] Both methods were linear from 25 to 200 μM (method one R^2 = 0.998, method two R^2 = 0.999).

Cell Culture—Stably transfected hASBT-Madin–Darby canine kidney (MDCK) cells were cultured at 37°C, 90% humidity, and 5% CO_2, as previously described.[21] Cells were fed every 2 days with DMEM fortified with 10% FBS, 50 units/mL penicillin, and 50 μ g/mL streptomycin. Geneticin (1 mg/mL) was added to maintain selection pressure. Cells were passaged after reaching 90% confluency (approximately every 4 days). Stably transfected hNTCP-human embryonic kidney (HEK) cells were cultured in a similar manner, with the addition of 1% nonessential amino acids to the fortified DMEM.[22] When 90% confluent, cells were seeded at a density of 0.6 million cells/well in 12-well plates (ASBT-MDCK cells) or at a density of 0.3 million cells/well in 24-well plates (NTCP-HEK). One day after seeding and 15 h prior to uptake studies, ASBT-MDCK cells were induced with 10 mM sodium butyrate. For both inhibition and uptake studies, three replicates were used for each donor concentration.

Inhibition of ASBT and NTCP—Both ASBT-MDCK and NTCP-HEK cells were exposed to donor solution 2 days after seeding. Inhibition donor solutions consisted of Hank's balanced salt solution (HBSS) in the presence of 2.5 μM native bile acid taurocholate. Inhibition donor solutions were spiked with 0.5 μ Ci/mL [^3H] taurocholate.

Cells were washed three times with HBSS and exposed to donor solution. After incubation at 37°C (10 min for hASBT-MDCK cells and 5 min for hNTCP-HEK cells, periods of linear uptake for these transfected cell lines), wells were rinsed three times with cold sodium-free buffer (SFB). In SFB, sodium chloride was replaced with 137 mM tetraethylammonium chloride. Cells were lysed using ACN (300 μL for MDCK cells and 150 μL for HEK cells)

and were left to evaporate at room temperature for 3 h. Wells were extracted with 1:1 ACN:water and counted for radioactivity using a LS6500 liquid scintillation counter (Beckmann Instruments, Inc., Fullerton, California).

Resulting data were fitted to a modified Michaelis–Menten competitive inhibition equation to regress for compound K_i . No weighting was used, and regression was performed using Phoenix WinNonlin (Pharsight, St. Louis, Missouri). This modified equation (Eq. (1)) accounts for aqueous boundary layer permeability, as previously described[23]

$$V=\frac{P_{\mathrm{ABL}}\left(\frac{V_{\max}}{K_{\mathrm{m}}(1+I/K_i)+S}+P_{\mathrm{p}}\right)}{P_{\mathrm{ABL}}+\frac{V_{\max}}{K_{\mathrm{m}}(1+I/K_i)+S}+P_{\mathrm{p}}}S \quad (1)$$

where V is taurocholate flux, P_{ABL} is aqueous boundary layer permeability (measured previously as 1.5×10^{-4} cm/s[24]), S is taurocholate concentration (i.e., 2.5 μM), and P_{p} is passive taurocholate permeability. K_{m} was set as 5.03 μM for ASBT inhibition and 5.31 μM for NTCP inhibition, determined from historic data.[25,26] P_{p} was determined by taurocholate uptake in SFB on the same occasion, measured using a saturating concentration of 200 μM.

Uptake of CA-sar-TFMA by ASBT and NTCP—Uptake studies were similar to inhibition studies, except that donor solutions consisted of 0–200 μM CA-sar-TFMA in either HBSS or SFB without taurocholate. Compound uptake in SFB was used to determine sodium-independent passive permeability, since both ASBT and NTCP are sodium-dependent uptake transporters. Cells were initially washed three times with either HBSS or SFB (consistent with donor), then exposed to donor solution and rinsed as described above. Extracts after cell lysing were stored at −80°C in silanized centrifuge tubes until analysis by liquid chromatography/tandem-mass spectrometry (LC/MS/MS). Taurocholate $V_{\max}$ was estimated using a saturating concentration of 200 μM on each study occasion. Taurocholate donor solutions were spiked with 0.5 μ Ci/mL [^{3}H] taurocholate.

Resulting uptake data were fitted to a modified Michaelis–Menten equation and regressed for $V_{\max}$ and K_{m} (Eq. (2)).

$$V=\frac{\mathrm{P}_{\mathrm{ABL}}\left(\frac{V_{\max}}{K_{\mathrm{m}}+S}+P_{\mathrm{p}}\right)}{P_{\mathrm{ABL}}+\frac{V_{\max}}{K_{\mathrm{m}}+S}+P_{\mathrm{p}}}S \quad (2)$$

$$V=\frac{P_{\mathrm{ABL}}P_{\mathrm{p}}}{P_{\mathrm{ABL}}+P_{\mathrm{p}}}S \quad (3)$$

HBSS uptake data (i.e., total uptake) were fitted using Eq. (2). V is substrate flux, P_{ABL} is 1.5×10^{-4} cm/s, as defined above, and P_{p} is passive permeability. P_{p} was estimated using Eq. (3) and SFB uptake data (i.e., sodium-independent uptake). After regression, $V_{\max}$ was normalized against the $V_{\max}$ of taurocholate on the same occasion, to account for variability in transporter expression. The resulting $V_{\max}$ is expressed as normVmax.

Stability of CA-sar-TFMA—Five micromolar of CA-sar-TFMA was incubated in 1 mL simulated intestinal fluid (SIF) with pancreatic enzymes, rat plasma, rat liver s9 fraction (1 mg/mL) with 1 mM nicotinamide adenine dinucleotide phosphate (NADPH) in Dulbecco's phosphate buffered saline (DPBS), and 0.1 M HCl to simulate stomach conditions (n = 3 for each). SIF, prepared according to the previously modified USP28 method,[27] consisted of 0.2 M NaOH, 6.8 g/L monobasic potassium phosphate, and 10 g/L pancreatin, adjusted to pH 7.5. In each of these studies, 1 mL solutions was incubated at 37°C before adding CA-sar-TFMA to start the experiment, yielding 5 μM CA-sar-TFMA. At time t = 0 and 4 h, 100 μL of CA-sar-TFMA in stability media was removed and added to 400 μL of cold ACN. Samples were centrifuged at 12,000g for 5 min, stored at −80°C, and then analyzed by LC/MS/MS.

CGH, a bacterial bile-acid deconjugating enzyme, was used to simulate conditions in the colon. CGH is found in small amounts in the terminal ileum and more abundantly in the colon. Stability of CA-sar-TFMA was evaluated in CGH from *Clostridium perfringens*. Previously, CA-lys-TFA was shown to be susceptible to deconjugation by CGH.[15] Ten millimolar mercaptoethanol, 1 mM ethylenediaminetetraacetic acid, and CA-sar-TFMA were added to 5 mM sodium acetate buffer at pH 5.6 (n = 3), yielding 2 mM CA-sar-TFMA.[28] After incubation at 37°C, the study was started by adding 15 U CGH. The stability of CA-lys-TFA was examined in parallel under the same conditions for comparison. Hundred microliters of samples was removed at t = 0, 15 min, 30 min, 1 h, 2 h, 3 h, and 4 h and diluted with 400 μL cold ACN. Samples were centrifuged at 12,000g for 5 min and analyzed by LC/MS/MS.

CA-sar-TFMA Solubility in Buffer—Five milligrams of compound was added to silanized centrifuge tubes containing 100 μL phosphate buffer at pH 6.8 (n = 3), shaken, and left overnight at room temperature. Subsequently, tubes were centrifuged at 12,000g for 5 min. Supernatant was diluted 10,000-fold with 1:1 ACN:water and analyzed by LC/MS/MS.

In Vitro ^{19}F MR Phantom Imaging—To evaluate the ^{19}F imaging signal intensity of CA-sar-TFMA, 30 mM of CA-sar-TFMA and 30 mM of CA-lys-TFA dissolved in methanol were imaged adjacent to one another on the same occasion in 2-mL glass vials (12-mm diameter; National Scientific, Rockwood, Tennessee).

Oral Disposition Characterization of CA-sar-TFMA: Pilot Study—All the animal studies were approved by the Institution Animal Care and Use Committee of both the University of Maryland School of Medicine and the Research and Development Committee at the VA Maryland Health Care System, in accordance with the *Guide for the Care and Use of Laboratory Animals* prepared by the U.S. National Academy of Sciences.[29] Six male C57BL/6 mice (average age 20.6 weeks, average weight 26.8 g) were purchased from Jackson Laboratories (Bar Harbor, Maine). Mice were housed with free access to water and standard mouse chow in a pathogen-free environment with a 12:12-h light/dark cycle for 1 week prior to experiments.

After an overnight fast, mice were gavaged with 150 mg/kg CA-sar-TFMA in vehicle [60% polyethylene glycol (PEG)400 and 40% DPBS, 8.33 μL per g mouse body weight]. Mice 1–

5 were maintained in the fasted state, and anesthetized at 7 h after dosing with ketamine/xylazine and exsanguinated by intracardiac puncture. Blood was collected into heparinized tubes and centrifuged at 12,000*g* for 10 min. Supernatants were analyzed by LC/MS/MS. Additionally, liver and gallbladder were removed and homogenized on ice with a glass tissue homogenizer (Duall size-21; Kimble Chase Life Science, Vineland, New Jersey). Imaging agent was extracted with 75% ACN in water (800 μL for liver and 300 μL for gallbladder). Extracts were centrifuged at 12,000*g* for 10 min and analyzed by LC/MS/MS.

Murine Gallbladder Imaging—After fasting and gavage as described above, mouse 6 was anesthetized with ketamine/xylazine by intraperitoneal (i.p.) catheter injection and subjected to ^{1}H MRI at 6.2 h after dosing. ^{19}F MRI was performed 6.7 h after dosing (1.5 h total ^{19}F acquisition time). Approximately every 30 min throughout imaging, maintenance doses of ketamine/xylazine were infused through the i.p. catheter. The mouse remained in the MRI machine for 2 h, including coil tuning time and ^{1}H and ^{19}F signal acquisition time. A 30 mM phantom of CA-sar-TFMA dissolved in methanol in a short glass NMR tube (5-mm diameter) was imaged alongside the mouse on the same occasion. After imaging, mouse euthanasia and tissue harvesting proceeded as described above. Tissues were analyzed by LC/MS/MS.

Asbt Knockout Mice—Asbt-deficient (*Slc10a2*$^{-/-}$) mice were obtained from a colony maintained at the Wake Forest School of Medicine. Four knockout mice (age 46.2 ± 3.3 weeks, weight 27.0 ± 1.4 g) and four WT littermates (age 43.8 ± 2.3 weeks, weight 29.5 ± 1.3 g) were fasted overnight and gavaged with 150 mg/kg CA-sar-TFMA in vehicle (3:2 PEG:DPBS). Gallbladder, liver, and plasma samples were collected at 7 h after dosing, and tissues were processed as described above and analyzed by LC/MS/MS.

Magnetic Resonance Imaging—All *in vitro* and *in vivo* MRI data were acquired using identical parameters, as described previously[18] (i.e., phantom and animal experiments used identical ^{19}F and ^{1}H parameters). Briefly, MRI experiments were performed on a Bruker BioSpec 70/30USR Avance III 7T horizontal bore MR scanner (Bruker Biospin MRI GmbH, Ettlingen, Germany) with a BGA12S gradient system and used Bruker ParaVision 5.1 software for acquisition and processing. The coil was a Bruker 40-mm ^{19}F/^{1}H dual-tuned linear volume coil that transmitted and received radiofrequency signals at 300.28 MHz for ^{1}H and 282.55 MHz for ^{19}F nuclei. Multislice ^{1}H MR images used an acquisition time of 7 min and 15 s using a RARE (rapid acquisition with relaxation enhancement) sequence in the cross view of the phantom or animal body. ^{1}H MRI employed repetition time 2200 ms, RARE factor 8, field of view 4×4 cm^2, echo time 8.9 ms, slice thickness 1.0 mm, matrix size 266 × 266, number of averages 6, and in-plane resolution 150 × 150μM^2. ^{19}F images were acquired with a FLASH (fast low angle shot) sequence in an identical region to ^{1}H MRI. ^{19}F acquisition time was 1 h and 30 min. Parameters were the same as ^{1}H MRI, but with repetition time 220 ms, echo time 3.078 ms, in-plane resolution 1.25 × 1.25 mm^2, matrix size 32 × 32, slice thickness 4.0 mm, number of averages 768, and flip angle = 30°. The flip angle was optimized using the T1 relaxation time of the phantom. For the *in vivo* mouse imaging experiment, the phantom was a 5-mm diameter shortened glass NMR tube containing 30 mM CA-sar-TFMA dissolved in methanol.

CA-sar-TFMA concentration in the gallbladder of mouse 6 was calculated by comparing the mean signal intensity in the region of interest (ROI) identified in the gallbladder to the mean signal intensity in the phantom ROI imaged next to the mouse body. In each case, the ROI was drawn to exclude the edges of phantom and gallbladder, so that signal intensity calculation did not suffer from a partial volume edge effect due to the image resolution. Mean signal intensity was calculated with Bruker ParaVision 5.1. The limit of quantification of ^{19}F signal for this method was previously determined to be 6.82 mM,[18] which corresponds to the noise magnitude of an ROI on the image periphery plus 2.5-times its standard deviation. Using this method, there is greater than 99% confidence that voxels with concentrations above this limit represent real ^{19}F signal, and not noise.[30]

Medical Image Processing, Analysis and Visualization software (MIPAV v7.0.1; CIT, NIH, Bethesda, Maryland) was used to generate a color ^{19}F MR image of mouse 6 and adjacent phantom. The image threshold used was 0.7 on a scale where the strongest signal (in red) was 1.0.

LC/MS/MS Analysis—CA-sar-TFMA concentrations, as well as CA-lys-TFA and cholic acid from CGH stability testing, were quantified with LC/MS/MS using a Waters Acquity UPLC system with triple quadrupole detector (Waters Corporation, Milford, Massachusetts). The column used was a Waters Acquity UPLC Ethylene Bridged Hybrid C8 1.7 μM 2.1 × 50 mm^2 column (0.4 mL/min flow rate, 10 μL injection volume). CA-sar-TFMA, CA-lys-TFA, and cholic acid were quantified with negative electrospray ionization, each employing a multiple reaction monitoring method. For CA-sar-TFMA, the transition 603.53 to 213.12 Da was monitored (dwell time 0.1 s, cone voltage 65 V, collision energy 36 V). For CA-lys-TFA, the transition 631.31–241.07 Da was monitored (dwell time 0.1 s, cone voltage 70 V, collision energy 40 V). For cholic acid, the transition 407.09–343.24 Da was monitored (dwell time 0.1 s, cone voltage 70 V, collision energy 34 V). For each method, the eluent used was a combination of water with 0.1% formic acid (A) and ACN with 0.1% formic acid (B). The gradient expressed as% B was as follows: initially 50% until 0.5 min, then increased to 95% at 1.5 min, decreased to 50% at 1.7 min, and maintained at 50% until 2.0 min. The methods were linear between 10 and 2000 nM (CA-sar-TFMA, R^2 = 0.9995; CA-lys-TFA, R^2 = 0.9998; cholic acid, R^2 = 0.9931).

Statistical Analysis—Error shown in the text and figures is standard error of the mean throughout. The Student's paired *t*-test was used to analyze data resulting from *in vitro* stability assays, whereas the Student's unpaired *t*-test was used to evaluate knockout versus WT mouse data. A *p* value of 0.05 or lower was considered significant.

Results

Synthesis of CA-sar-TFMA

CA-sar-TFMA was successfully synthesized. When stained with 10% (w/v) phosphomolybdic acid in EtOH, TLC showed a single spot that did not move using a solvent of 10% methanol in DCM. MS analysis showed appropriate peaks of [M+23] 627.3 and [M–1] 603.4, and confirmed that no cholic acid was present. The first HPLC method had R_T = 2.94 min, whereas the second showed R_T = 3.62 min (purity 99.0%).

^{13}C NMR and two-dimensional analysis showed two rotational isomers of CA-sar-TFMA. Thus, like other drugs, for example, valsartan,[31] CA-sar-TFMA appears to have two different rotational states around a tertiary amide bond that yields split peaks for carbon atoms. Tertiary amide bonds often give rise to rotamers because of the inherent flexibility of the bond, and the inability to form stabilizing hydrogen bonds. Rotamers were present in almost equal amounts, with rotamer A (designated below) slightly more abundant than rotamer B. ^{13}C NMR in DMSO-d_6, rotamer A: δ 12.78, 17.54, 23.06, 23.27, 26.64, 27.73, 28.97, 29.60, 30.84, 31.50, 34.82, 35.31, 35.46, 35.76, 38.07, 39.93, 40.00, 41.80, 41.95, 46.58, 46.20, 46.91, 47.56, 70.87, 71.46, 117.72, 156.74, 171.45, 173.33. ^{13}C NMR in DMSO-d_6, rotamer B: δ 12.78, 17.54, 23.06, 23.27, 26.64, 27.64, 28.97, 29.60, 30.84, 31.27, 34.82, 35.31, 35.46, 35.76, 39.93, 40.00, 41.80, 41.95, 45.64, 46.20, 46.91, 50.10, 66.67, 70.87, 71.46, 114.86, 156.94, 171.87, 174.10. Hence, carbon atoms affected by rotamer formation were carbons 16, 22, and 24 of the cholic acid scaffold, along with all of the carbon atoms on the conjugated side chain (i.e., carbons 25–30). ^{19}F NMR spectra of compound 5 (Fig. 1) and CA-sar-TFMA confirm the presence of two isomers both CA-sar-TFMA and its synthetic precursor (Supporting Information Fig. S1).

Inhibition of ASBT and NTCP

CA-sar-TFMA was a potent inhibitor of both ASBT and NTCP. Figure 2 shows the results of the inhibition of taurocholate uptake by CA-sar-TFMA in stably transfected ASBT-MDCK cells (a) and stably transfected NTCP-HEK cells (b). Regression analysis showed ASBT K_i = 21.5 ± 4.0 μM and NTCP K_i = 2.64 ± 0.55 μM.

Uptake of CA-sar-TFMA by ASBT and NTCP

Figure 3 shows the results of uptake of CA-sar-TFMA by ASBT (a) and NTCP (b). Regression analysis showed ASBT K_m = 73.2 ± 7.0 μM, passive permeability (P_p) = 2.10 × 10^{-} cm/s, and normVmax (normalized to taurocholate Vmax on the same occasion) = 1.50. For NTCP uptake, K_m = 2.19 ± 0.63 μM, P_p = 0.43 × 10^{-7} cm/s, and normVmax = 0.24. For comparison, in the same cell lines the native bile acid taurocholate has K_m values of 5.03[32] and 5.31 μM[33] for ASBT and NTCP, respectively.

Stability of CA-sar-TFMA

In Figure 4, results are shown from stability analysis of CA-sar-TFMA in 0.1 M HCl, rat plasma, rat liver s9 fraction with 1 mM NADPH, and SIF. The novel bile acid showed favorable stability in each environment with no evidence of degradation. Using the Student's paired *t*-test, concentrations of CA-sar-TFMA at *t* = h were not significantly different from starting concentrations. The lowest one-tailed *p* value observed was 0.30.

In Figure 5, results of CA-sar-TFMA stability against CGH are shown. After 4 h, 38.9 ± 0.2% of CA-lys-TFA remained, with 20.5 ± 0.3% release of cholic acid (shown in a). In contrast, 103.9 ± 2.9% of CA-sar-TFMA remained, with no release of cholic acid (shown in b). Therefore, CA-sar-TFMA showed improved *in vitro* stability over CA-lys-TFA in response to bile acid deconjugation by CGH. Presumably, the tertiary amide bond linkage to cholic acid in CA-sar-TFMA afforded this improved stability compared with CA-lys-TFA, which possesses a secondary amide bond linkage.

CA-sar-TFMA Solubility in Buffer

Solubility in phosphate buffer at pH 6.8 was measured to be 33.5 ± 1.6 mM, above the ^{19}F limit of quantification of approximately 5 mM trifluorinated compound (i.e., 15 mM fluorine atoms) determined previously with the same equipment and MRI parameters used here.[18]

In Vitro ^{19}F MR Phantom Imaging

An MR phantom image of 30 mM CA-sar-TFMA adjacent to 30 mM CA-lys-TFA is shown in Figure 6. Each is dissolved in methanol in 2-mL glass vials. This figure demonstrates that, although the CA-sar-TFMA has a split flourine peak, the total signal intensity is similar to that of CA-lys-TFA, which did not exhibit a split peak of its three equivalent fluorine atoms. CA-sar-TFMA peak splitting did not appear to affect MRI signal intensity, as anticipated since peak split only spanned 0.045 ppm or less. The ^{19}F average ROI signal intensity of both CA-sar-TFMA and CA-lys-TFA were identical, at 2.66 each (arbitrary units).

Oral Disposition Characterization of CA-sar-TFMA: Pilot Study

CA-sar-TFMA showed high targeting to the mouse gallbladder at 7 h after oral dosing. Results are shown in Table 1. Liver and gallbladder concentrations of CA-sar-TFMA were calculated by assuming an organ density of 1 g/mL. Average gallbladder concentration was 18.4 ±1.6 mM. In contrast, accumulation in the liver and plasma were on average at least 1000-fold lower than in gallbladder. Average liver concentration was 14.5 ± 0.6 μM, whereas average plasma concentration was 1.40 ± 0.14 μM. Gallbladder concentrations were above the ^{19}F MRI limit of detection for a trifluorinated compound, as previously defined,[18] and liver and plasma concentrations were below the limit of detection.

Murine Gallbladder Imaging

Mouse 6 underwent MR imaging at 6.2–8.2 h after oral gavage of 150 mg/kg CA-sar-TFMA. In Figure 7, a high concentration of CA-sar-TFMA was visualized in the gallbladder by ^{19}F MRI (identified anatomically by its corresponding ^{1}H image). Compound concentration was calculated by normalizing the average intensity of the gallbladder ROI to that within the phantom, and was determined to be 34.2 mM. After euthanasia, mouse gallbladder concentration was analyzed by LC/MS/MS to be 14.8 mM. This 2.3-fold lower concentration agrees with our previous observations that LC/MS/MS-based gallbladder concentrations are typically 2.7(±0.8)-fold lower than those observed by MRI due to animal handling after imaging.[18] Since gallbladder emptying is a mechanical process, we attributed this previously observed difference (on two independent occasions) in measured concentrations to partial emptying of the gallbladder as a consequence of animal handling (e.g., removal from the scanner, transport to a surgical facility, and the application of additional sedation before harvesting of tissue).[18] Corresponding liver and plasma CA-sar-TFMA concentrations for mouse 6 were much lower than those in gallbladder; liver and plasma CA-sar-TFMA concentrations were 7.66 and 0.87 μM, respectively.

Asbt Knockout Mice

Knockout and WT mice (n = 4) each were gavaged with 150 mg/kg CA-sar-TFMA and euthanized after 7 h. CA-sar-TFMA concentrations were determined by LC/MS/MS

analysis. In Figure 8, CA-sar-TFMA accumulated at 16.1-fold higher concentrations in WT mice gallbladders than in knockout mice gallbladders (6.61 ± 0.98 mM vs. 0.41 ± 0.14 mM, $p = 0.0008$). As in the pilot disposition study, liver and plasma levels of CA-sar-TFMA were much lower than in gallbladder. Liver concentration was 4.97 ± 1.47 μM in WT mice and 0.90 ± 0.03 μM in knockout mice ($p = 0.02$). Plasma concentration was 3.80 ± 4.15 μM in WT mice and 0.22 ± 0.09 μM in knockout mice ($p = 0.36$). The significantly reduced levels of CA-sar-TFMA observed in Asbt knockout mice are likely due to passive absorption, in agreement with the low absorption of CA-sar previously described in studies of vascularly-perfused closed loops of rat duodenum.[34]

Discussion

The objective of this study was to design a fluorinated bile acid resistant to bacterial enzyme deconjugation, to test its *in vitro* stability, transport properties, and gallbladder accumulation after oral dosing. We also examined the agent's ^{19}F imaging characteristics, and its ability to differentially accumulate in the gallbladder in WT mice versus mice with known impaired intestinal bile acid transport (*Slc10A2*$^{-/-}$ mice). We chose to approach this objective by designing a trifluorinated bile acid structurally similar to cholylsarcosine.

Batta et al.[35] showed that bile acids conjugated with a tertiary amide bond at the C-24 position (i.e., sarcosine or N-methyl taurine conjugated) are resistant to deconjugation by CGH. After this finding, cholylsarcosine, a conjugate of cholic acid and sarcosine, was developed as a potential conjugated bile acid replacement.[36,37] Cholylsarcosine mimics the transport of native bile acids in the enterohepatic circulation, and is not metabolized in the body by deconjugation or dehydroxylation.[38] Cholylsarcosine possesses a single negative charge in the region that promotes uptake by ASBT.[39] Based on these characteristics, cholylsarcosine has been explored for use as a bile acid replacement in short bowel syndrome to enhance lipid solubilization[40] and tested as an agent to reduce intestinal bacterial overgrowth in cirrhotic rats.[41] Recently, a ^{11}C-radiolabeled form was investigated for use in measuring the hepatic excretion of bile acids.[42]

CA-sar-TFMA was designed as a potential ^{19}F-MRI agent that would emulate the stability of cholylsarcosine. CA-sar-TFMA is structurally similar to cholylsarcosine, but with the addition of a trifluoro-N-methyl-acetamide group. This group yields the target CA-sar-TFMA compound with three equivalent fluorine atoms, which we previously showed to be sufficient for ^{19}F MRI of a fluorinated bile acid.[18]

CA-sar-TFMA was synthesized and tested against the sodium-dependent bile acid uptake transporters, ASBT and NTCP. CA-sar-TFMA was a potent substrate and inhibitor of both transporters. Four-hour stability testing of CA-sar-TFMA in HCl, SIF, rat plasma, rat liver s9 fraction, and CGH showed no significant compound degradation. Preliminary *in vivo* testing showed that an oral dose of 150 mg/kg CA-sar-TFMA accumulates in the mouse gallbladder above the minimum required for quantification by ^{19}F MRI (6.82 mM[18]), and is present in much lower concentrations in the liver and plasma. CA-sar-TFMA was successfully imaged in the mouse gallbladder by ^{19}F MRI, and showed a 16.1-fold difference in gallbladder accumulation in WT compared with Asbt-deficient mice. These *in*

vivo findings suggest that the other major carriers in the en-terohepatic circulation, OSTα-OSTβ and BSEP, also efficiently transport CA-sar-TFMA. However, minor roles cannot be excluded for other carriers such as members of the OATP family.

The *in vitro* transport properties of CA-sar-TFMA were characterized using cells expressing the human orthologs of NTCP and ASBT, whereas the *in vivo* transport was examined in mice. Studies using membrane vesicles or transporter-transfected cells have been used to examine the bile acid transporter properties of NTCP/Ntcp and ASBT/Asbt from individual species, though direct comparisons have not typically been performed in the same study. In general, the inter-species bile acid transport differences are small for both carriers. Human ASBT and murine Asbt have 81% identity and 88% similarity, whereas human NTCP and murine NTCP have 78% identity and 85% similarity (computed using the Basic Local Alignment Search Tool, NCBI-BLAST®[43]).

Compared with CA-lys-TFA, CA-sar-TFMA has similar ASBT and NTCP transport properties. CA-lys-TFA and CA-sar-TFMA are substrates of both transporters, with a higher affinity for NTCP than ASBT (CA-lys-TFA ASBT and NTCP K_m values were 39.4 ± 23.8 and 8.99 ± 2.79 μM, respectively, whereas CA-sar-TFMA ASBT and NTCP K_m values were 73.2 ± 7.0 and 2.19 ± 0.63 μM).[15] Although CA-sar-TFMA K_m and K_i values were similar for NTCP (2.19 vs. 2.64 μM), these values differed more than three-fold for ASBT (73.2 vs. 21.5 μM). We speculate that this K_m versus K_i difference may result from binding of CA-sar-TFMA to a region of ASBT that interferes with binding of taurocholate but does not participate in uptake of CA-sar-TFMA. Such an inhibition-only binding site could account for CA-sar-TFMA being a more potent inhibitor than substrate for ASBT. Both CA-lys-TFA and CA-sar-TFMA accumulate in the mouse gallbladder at concentrations considerably greater than those in liver and plasma, and both accumulate much more in WT gallbladder compared with Asbt-deficient gallbladder. Importantly, unlike CA-lys-TFA, CA-sar-TFMA was resistant to deconjugation by CGH *in vitro*.

Future studies to investigate the impact of the increased *in vitro* stability of CA-sar-TFMA will include a more comprehensive *in vivo* murine pharmacokinetic analysis and *in vivo* half-life, compared with that of CA-lys-TFA. Additionally, changes in CA-sar-TFMA and CA-lys-TFA pharmacokinetics when mice are pretreated with antibiotics will be examined. If resistance to hydrolysis by CGH is the major determinant of the prolonged half-life of CA-sar-TFMA compared with CA-lys-TFA, we anticipate that antibiotic pretreatment will not alter the half-life of CA-sar-TFMA but will increase that of CA-lys-TFA. Overall, the present studies identify CA-sar-TFMA as a novel ^{19}F MRI probe that warrants further study for non-invasive, *in vivo* diagnosis of abnormal bile acid transport.

Supplementary Material

Refer to Web version on PubMed Central for supplementary material.

Acknowledgments

This work was supported by the National Institutes of Health, National Institute of Diabetes and Digestive and Kidney Diseases (grants DK-093406, DK-067872, DK-047987, and DK-081479), National Cancer Institute (grant CA-120407), and the Food and Drug Administration (collaborative agreement U01FD004320).

References

1. Hofmann AF, Molino G, Milanese M, Belforter G. Description and simulation of a physiological pharmacokinetic model for the metabolism and enterohepatic circulation of bile acids in man. Cholic acid in healthy man. J Clin Invest. 1983; 71:1003–1022. [PubMed: 6682120]
2. Dawson PA. Role of the intestinal bile acid transporters in bile acid and drug disposition. Handb Exp Pharmacol. 2011; 201:169–203. [PubMed: 21103970]
3. Wedlake L, A'Hern R, Russell D, Thomas K, Walters JR, Andreyev HJ. Systematic review: The prevalence of idiopathic bile acid malabsorption (I-BAM) as diagnosed by SeHCAT scanning in patients with diarrhoea-predominant irritable bowel syndrome (IBS). Aliment Pharmacol Ther. 2009; 30:707–717. [PubMed: 19570102]
4. Smith MJ, Cherian P, Ruju GS, Dawson BF, Mahon S, Bardhan KD. Bile acid malabsorption in persistent diarrhoea. J R Coll Physicians Lond. 2000; 34:448–451. [PubMed: 11077656]
5. Williams AJ, Merrick MV, Eastwood MA. Idiopathic bile acid malabsorption—A review of clinical presentation, diagnosis, and response to treatment. Gut. 1991; 32:1004–1006. [PubMed: 1916479]
6. Sciarretta G, Fagioli G, Furno A, Vicini G, Cecchetti L, Grigolo B, Verri A, Malaguti P. ^{75}Se HCAT test in the detection of bile acid malabsorption in functional diarrhoea and its correlation with small bowel transit. Gut. 1987; 28:970–975. [PubMed: 3666565]
7. Wedlake L, Thomas K, Lalji A, Anagnostopoulos C, Andreyev HJ. Effectiveness and tolerability of colesevelam hydrochloride for bile-acid malabsorption in patients with cancer: A retrospective chart review and patient questionnaire. Clin Ther. 2009; 31:2549–2558. [PubMed: 20109999]
8. Hofmann AF, Mangelsdorf DJ, Kliewer SA. Chronic diarrhea due to excessive bile acid synthesis and not defective ileal transport: A new syndrome of defective FGF19 release. Clin Gastroenterol Hepatol. 2009; 7:1151–1154. [PubMed: 19665580]
9. Merrick MV, Eastwood MA, Anderson JR, Ross HM. Enterohepatic circulation in man of a gamma-emitting bile-acid conjugate, 23-Selena–25-Homotaurocholic Acid (SeHCAT). J Nucl Med. 1981; 23:126–130. [PubMed: 7057253]
10. Pedersen L, Arnfred T, Thaysen EH. Rapid screening of increased bile acid deconjugation and bile acid malabsorption by means of the glycine-l-(^{14}C) cholylglycine assay. Scand J Gastroenterol. 1973; 8:665–672. [PubMed: 4768311]
11. Brydon WG, Nyhlin H, Eastwood MA, Merrick MV. Serum 7 alpha-hydroxy-4-cholesten-3-one and selenohomocholyltaurine (Se-HCAT) whole body retention in the assessment of bile acid induced diarrhoea. Eur J Gastroenterol Hepatol. 1996; 8:117–123. [PubMed: 8723414]
12. Lenicek M, Duricova D, Komarek V, Gabrysova B, Lukas M, Smer-hovsky Z, Vitek L. Bile acid malabsorption in inflammatory bowel disease: Assessment by serum markers. Inflamm Bowel Dis. 2011; 17:1322–1327. [PubMed: 21058331]
13. Khalid U, Lalji A, Stafferton R, Andreyev J. Bile acid malabsorption: A forgotten diagnosis? Clin Med. 2010; 10:124–126. [PubMed: 20437979]
14. Vijayvargiya P, Camilleri M, Shin A, Saenger A. Methods for diagnosis of bile acid malabsorption in clinical practice. Clin Gastroenterol Hepatol. 2013; 11:1232–1239. [PubMed: 23644387]
15. Vivian D, Cheng K, Khurana S, Xu S, Whiterock V, Witter D, Lentz KA, Santone KS, Raufman JP, Polli JE. Design and characterization of a novel fluorinated magnetic resonance imaging agent for functional analysis of bile acid transporter activity. Pharm Res. 2013; 30:1240–1251. [PubMed: 23319170]
16. Yu JX, Kodibagkar VD, Cui W, Mason RP. ^{19}F: A versatile reporter for non-invasive physiology and pharmacology using magnetic resonance. Curr Med Chem. 2005; 12:819–848. [PubMed: 15853714]

17. Jiang ZX, Liu X, Jeong EK, Yu YB. Symmetry-guided design and fluorous synthesis of a stable and rapidly excreted imaging tracer for (19)F MRI. Angew Chem Int Ed Engl. 2009; 48:4755–4758. [PubMed: 19475598]
18. Vivian D, Cheng K, Khurana S, Xu S, Kriel EH, Dawson PA, Raufman JP, Polli JE. In vivo performance of a novel fluorinated magnetic resonance imaging agent for functional analysis of bile acid transport. Mol Pharm. 2014; 11:1575–1582. [PubMed: 24708306]
19. Dawson PA, Haywood J, Craddock AL, Wilson M, Tietjen M, Kluckman K, Maeda N, Parks JS. Targeted deletion of the ileal bile acid transporter eliminates enterohepatic cycling of bile acids in mice. J Biol Chem. 2003; 278:33920–33927. [PubMed: 12819193]
20. Vertzoni M, Archontaki H, Reppas C. Determination of intralumenal individual bile acids by HPLC with charged aerosol detection. J Lipid Res. 2008; 49:2690–2695. [PubMed: 18693215]
21. Balakrishnan A, Sussman DJ, Polli JE. Development of stably transfected monolayer overexpressing the human apical sodium-dependent bile acid transporter (hASBT). Pharm Res. 2005; 22:1269–1280. [PubMed: 16078136]
22. Leonhardt M, Keiser M, Oswald S, Kühn J, Jia J, Grube M, Kroemer HK, Siegmund W, Weitschies W. Hepatic uptake of the magnetic resonance imaging contrast agent Gd-EOB-DTPA: Role of human organic anion transporters. Drug Metab Dispos. 2010; 38:1024–8. [PubMed: 20406852]
23. Balakrishnan A, Polli JE. Deleterious effect of high transporter expression in the estimation of transporter kinetics. AAPS J. 2005; 7:R6224.
24. Balakrishnan A, Hussainzada N, Gonzalez P, Bermejo M, Swaan PW, Polli JE. Bias in estimation of transporter kinetic parameters from overexpression systems: Interplay of transporter expression level and substrate affinity. J Pharmacol Exp Ther. 2007; 320:133–144. [PubMed: 17038509]
25. Zheng X, Polli JE. Identification of inhibitor concentrations to efficiently screen and measure inhibition K_i values against solute carrier transporters. Eur J Pharm Sci. 2010; 41:43–52. [PubMed: 20553862]
26. Kolhatkar V, Polli JE. Structural requirements of bile acid transporters: C-3 and C-7 modifications of steroidal hydroxyl groups. Eur J Pharm Sci. 2012; 46:86–99. [PubMed: 22387310]
27. Vertzoni M, Fotaki N, Kostewicz E, Stippler E, Leuner C, Nicolaides E, Dressman J, Reppas C. Dissolution media simulating the intralumenal composition of the small intestine: Physiological issues and practical aspects. J Pharm Pharmacol. 2004; 56:453–462. [PubMed: 15099440]
28. Huijghebaert SM, Hofmann AF. Influence of the amino acid moiety on deconjugation of bile acid amidates by cholylglycine hydrolase or human fecal cultures. J Lipid Res. 1986; 27:742–752. [PubMed: 2876046]
29. Committee for the Update of the Guide for the Care and Use of Laboratory Animals; National Research Council. Guide for the care and use of laboratory animals. 8th. Washington DC: National Academies Press; 2011.
30. Srinivas M, Morel PA, Ernst LA, Laidlaw DH, Ahrens ET. Fluorine-19 MRI for visualization and quantification of cell migration in a diabetes model. Magn Reson Med. 2007; 58:725–734. [PubMed: 17899609]
31. Li F, Zhang H, Jiang L, Zhang W, Nie J, Feng Y, Yang M, Liu M. Dynamic NMR study and theoretical calculations on the conformational exchange of valsartan and related compounds. Magn Reson Chem. 2007; 45:929–936. [PubMed: 17876862]
32. Zheng X, Polli JE. Identification of inhibitor concentrations to efficiently screen and measure inhibition K_i values against solute carrier transporters. Eur J Pharm Sci. 2010; 41:43–52. [PubMed: 20553862]
33. Kolhatkar V, Polli JE. Structural requirements of bile acid transporters: C-3 and C-7 modifications of steroidal hydroxyl groups. Eur J Pharm Sci. 2012; 46:86–99. [PubMed: 22387310]
34. Chen X, Chen F, Liu S, Glaeser H, Dawson PA, Hofmann AF, Kim RB, Shneider BL, Pang KS. Transactivation of rat apical sodium-dependent bile acid transporter and increased bile acid transport by 1alpha,25-dihydroxyvitamin D3 via the vitamin D receptor. Mol Pharmacol. 2006; 69:1913–1923. [PubMed: 16481392]
35. Batta AK, Salen G, Shefer S. Substrate specificity of cholylglycine hydrolase for the hydrolysis of bile acid conjugates. J Biol Chem. 1984; 259:15035–15039. [PubMed: 6096355]

36. Schmassmann A, Angellotti MA, Ton-Nu HT, Schteingart CD, Marcus SN, Rossi SS, Hofmann AF. Transport, metabolism, and effect of chronic feeding of cholylsarcosine, a conjugated bile acid resistant to deconjugation and dehydroxylation. Gastroenterology. 1990; 98:163–174. [PubMed: 1688373]
37. Lillienau J, Schteingart CD, Hofmann AF. Physicochemical and physiological properties of cholylsarcosine. A potential replacement detergent for bile acid deficiency states in the small intestine. J Clin Invest. 1992; 89:420–31. [PubMed: 1371123]
38. Schmassmann A, Fehr HF, Locher J, Lillienau J, Schteingart CD, Rossi SS, Hofmann AF. Cholylsarcosine, a new bile acid analogue: Metabolism and effect on biliary secretion in humans. Gastroenterology. 1993; 104:1171–81. [PubMed: 7681796]
39. Swaan PW, Szoka FC Jr, Oie S. Molecular modeling of the intestinal bile acid carrier: A comparative molecular field analysis study. J Comput Aided Mol Des. 1997; 11:581–588. [PubMed: 9491350]
40. Heydorn S, Jeppesen PB, Mortensen PB. Bile acid replacement therapy with cholylsarcosine for short-bowel syndrome. Scand J Gastroenterol. 1999; 34:818–823. [PubMed: 10499484]
41. Lorenzo-Zúñiga V, Bartolí R, Planas R, Hofmann AF, Viñado B, Hagey LR, Hernández JM, Mañé J, Alvarez MA, Ausina V, Gassull MA. Oral bile acids reduce bacterial overgrowth, bacterial translocation, and endotoxemia in cirrhotic rats. Hepatology. 2003; 37:551–557. [PubMed: 12601352]
42. Frisch K, Jakobsen S, Sørensen M, Munk OL, Alstrup AK, Ott P, Hofmann AF, Keiding S. [N-methyl-^{11}C]cholylsarcosine, a novel bile acid tracer for PET/CT of hepatic excretory function: Radiosynthesis and proof-of-concept studies in pigs. J Nucl Med. 2010; 53:772–778. [PubMed: 22454486]
43. Altschul SF, Gish W, Miller W, Myers EW, Lipman DJ. Basic local alignment search tool. J Mol Biol. 1990; 215:403–410. [PubMed: 2231712]

Abbreviations used

ACN	acetonitrile
ASBT	the apical sodium-dependent bile acid transporter
BAM	bile acid malabsorption
BSEP	the bile salt export pump
CGH	choloylglycine hydrolase
DCM	dichloromethane
DMEM	Dulbecco's modified Eagle medium
DMF	dimethyl formamide
DPBS	Dulbecco's phosphate buffered saline
DMSO	dimethyl sulfoxide
EtOH	ethanol
FBS	fetal bovine serum
FGF	fibroblast growth factor
FLASH	fast low angle shot
HBSS	Hank's balanced salt solution
HBTU	hexaflourophos-phate

HCAT	homocholic acid-taurine
HEK	human embryonic kidney
HOBt	hydroxybenzotriazole
HSQC	heteronuclear single quantum coherence
IBS	irritable bowel syndrome
i.p	intraperitoneal
LC/MS/MS	liquid chromatography/tandem-mass spectrometry
MDCK	Madin–Darby canine kidney
MRI	magnetic resonance imaging
MRP2	the multidrug resistance-associated protein 2
MRP3	the multidrug resistance-associated protein 3
MS	mass spectrometry
NADPH	nicotinamide adenine din-ucleotide phosphate
NaOH	sodium hydroxide
NMR	nuclear magnetic resonance
NTCP	the Na^+/taurocholate cotransporting polypeptide
OATPs	the organic anion transporting peptides
OSTα-OSTβ	the organic solute transporters
PEG	polyethylene glycol
RARE	rapid acquisition with relaxation enhancement
ROI	region of interest
SFB	sodium-free buffer
SIF	simulated intestinal fluid with pancreatic enzymes
TEA	triethylamine
TFA	trifluoroacetic acid
TLC	thin-layer chromatography
WT	wild type

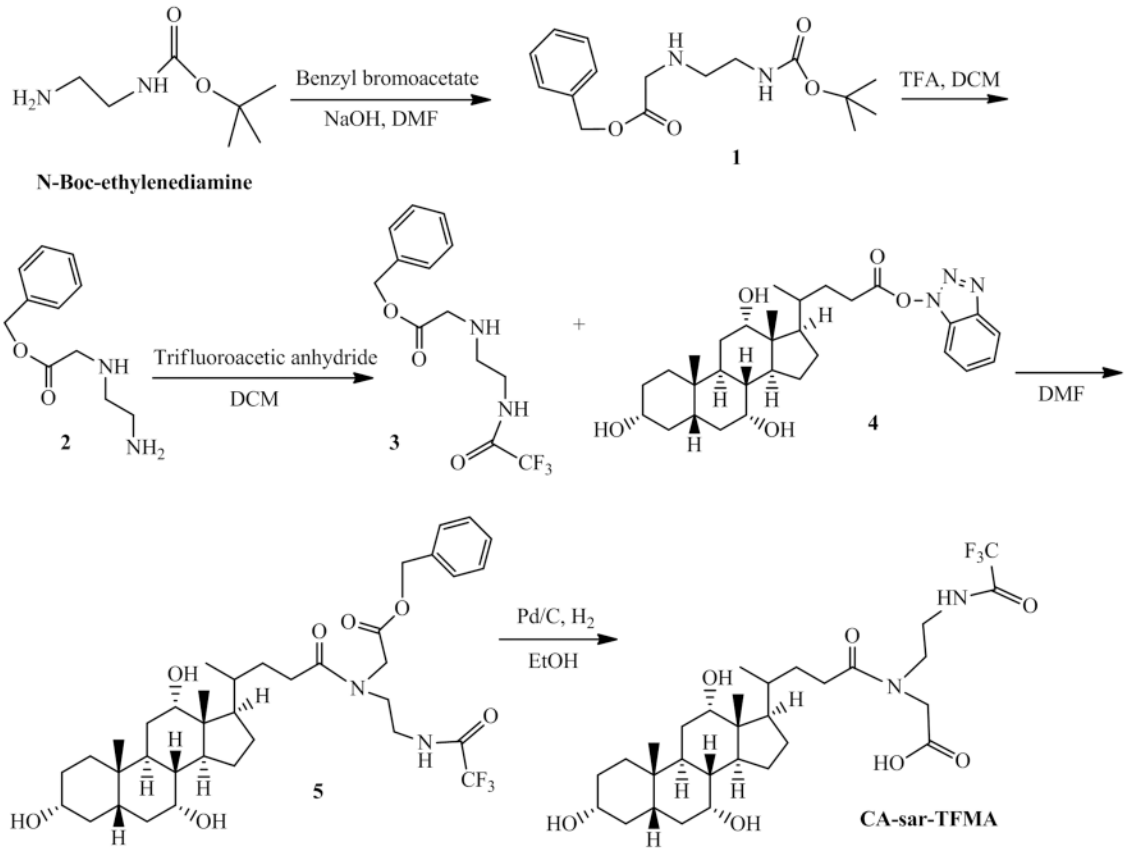

Figure 1.

Synthesis of CA-sar-TFMA. N-Boc-ethylenediamine was first reacted with benzyl bromoacetate, then the N-Boc group was removed with TFA. The free amine was trifluoroacetylated, and the resulting product was conjugated to an activated OBt ester form of cholic acid. To form the final product, the benzyl group in compound 5 was removed by catalytic hydrogenation.

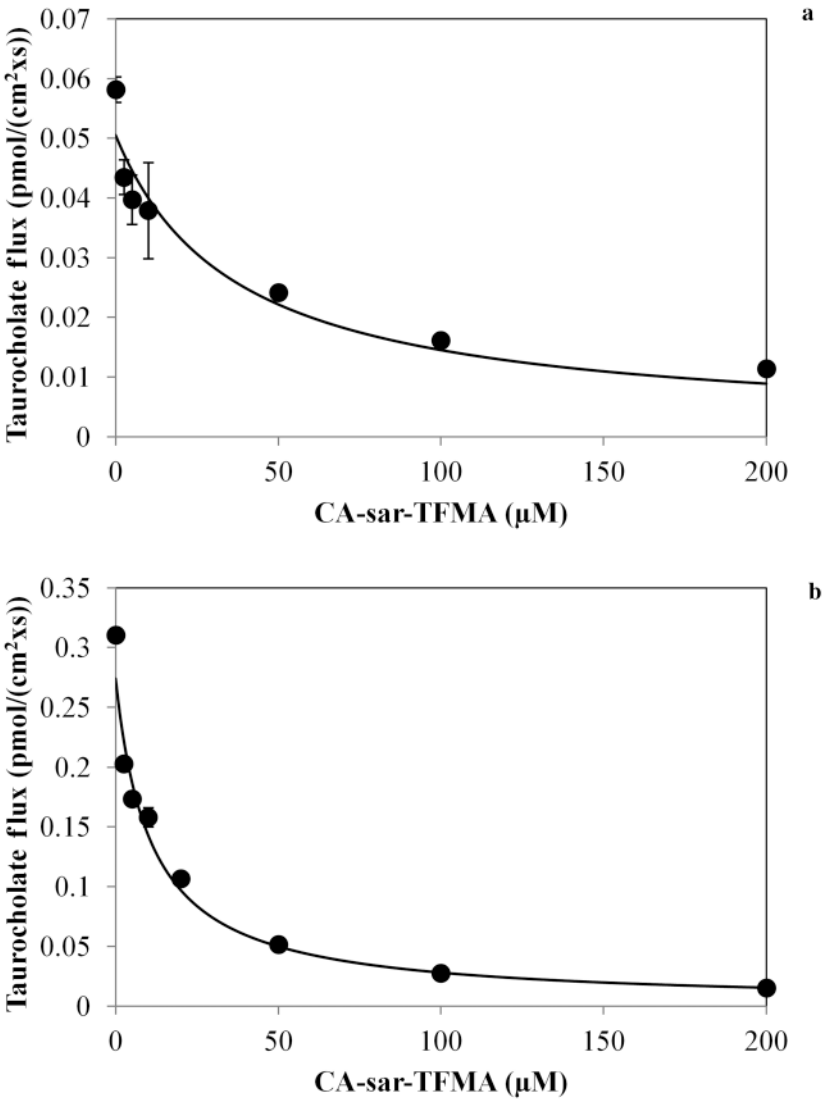

Figure 2.

Inhibition of taurocholate uptake by ASBT (a) and NTCP (b) by CA-sar-TFMA. Regression analysis showed ASBT K_i = 21.5 ± 4.0 μM and NTCP K_i = 2.64 ± 0.55 μM. Each point represents n = 3 samples.

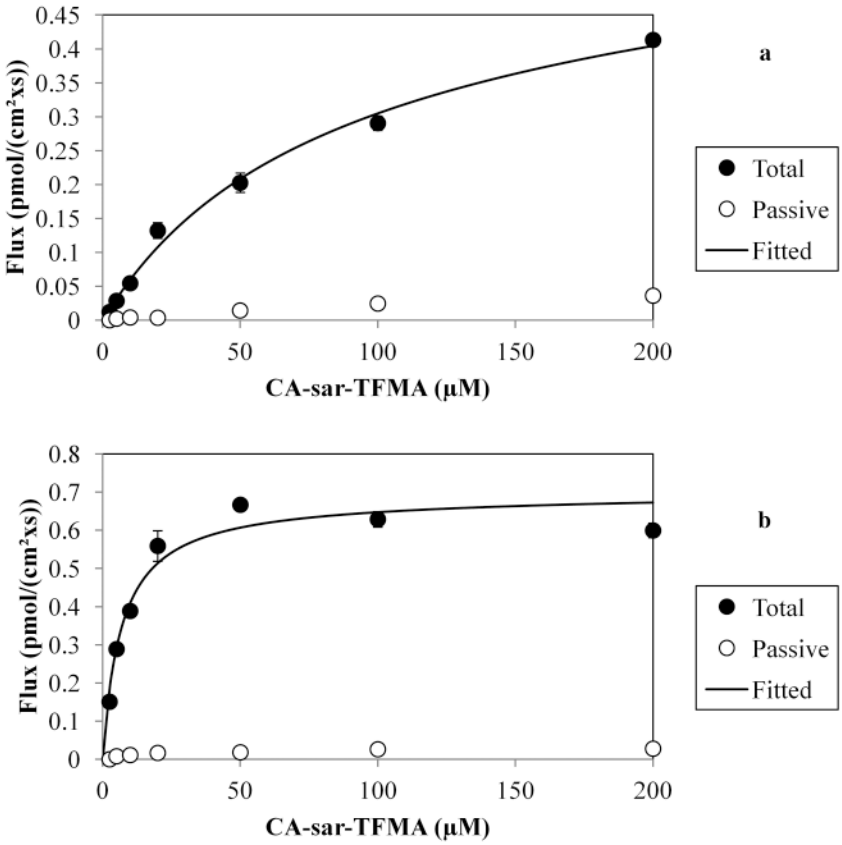

Figure 3.

Uptake of CA-sar-TFMA by ASBT (a) and NTCP (b). Regression analysis showed ASBT K_m = 73.2 ± 7.0 μM and NTCP K_m = 2.19 ± 0.63 μM. Each point represents n = 3 samples.

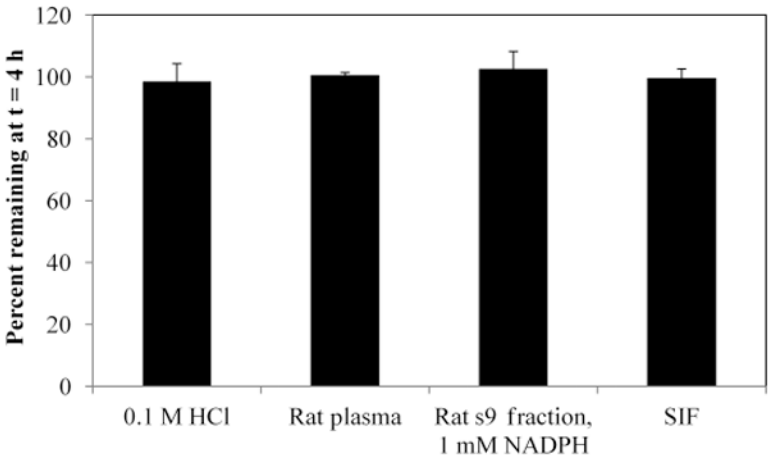

Figure 4.

In vitro stability of CA-sar-TFMA. Concentration of CA-sar-TFMA at $t = 4$ h was not different from initial concentration in 0.1 M HCl, rat plasma, rat s9 fraction with 1 mM NADPH, or SIF ($p > 0.3$ for Student's paired *t*-test). Each point represents $n = 3$ samples.

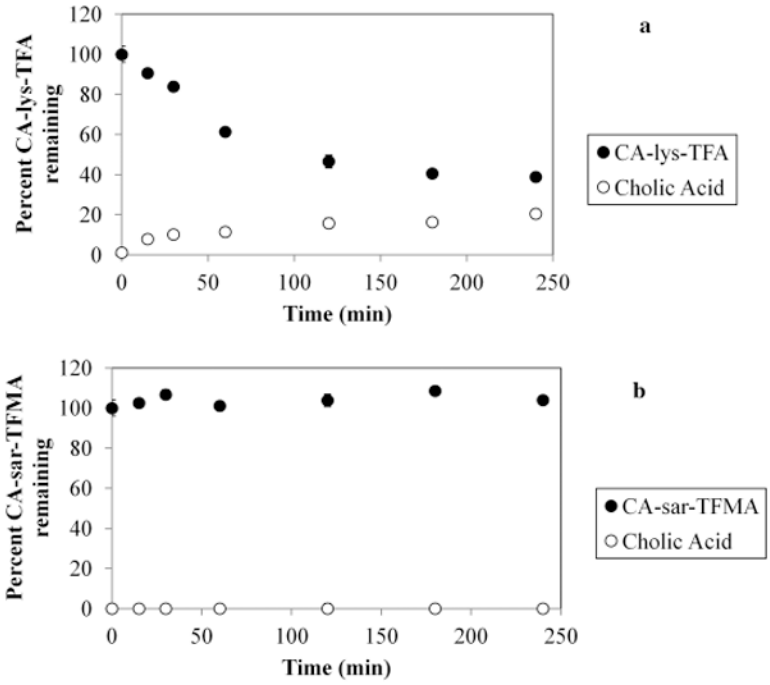

Figure 5.

Stability of CA-sar-TFMA (a) and CA-lys-TFA (b) in the presence of choloylglycine hydrolase. After 4 h, 103.9 ± 2.9% of CA-sar-TFMA remained, with no detectable release of cholic acid. In contrast, 38.9 ± 0.2% of CA-lys-TFA remained after 4 h, with 20.5 ± 0.3% release of cholic acid. Each point represents $n = 3$ samples.

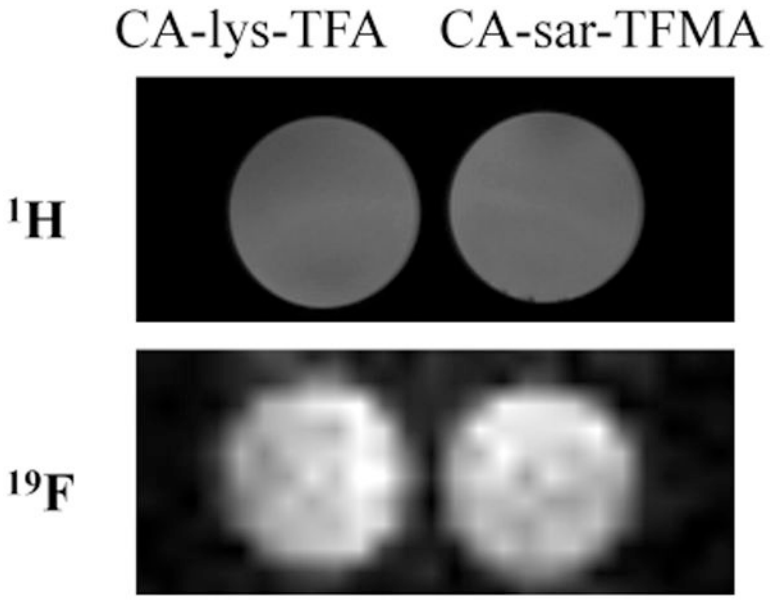

Figure 6.

^{1}H and ^{19}F MRI of fluorinated bile acids. 2-mL glass vials of 30 mM CA-lys-TFA and 30 mM CA-sar-TFMA were imaged adjacent to one another on the same occasion. Analysis of ^{19}F MR images using Bruker ParaVision 5.1 showed that CA-lys-TFA and CA-sar-TFMA phantoms provided identical average signal intensities. This equivalence in intensities reflects that both compounds contain three equivalent fluorines (i.e., possess identical number of fluorine atoms).

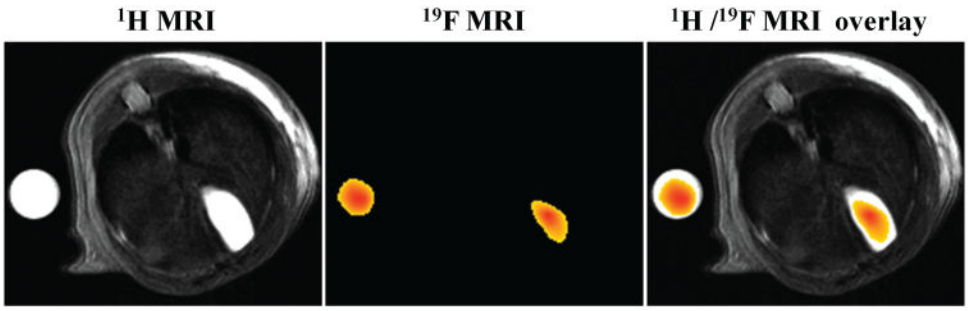

Figure 7.

CA-sar-TFMA *in vivo* MR images. The left-most panel shows a ^{1}H MR image of the cross section of mouse 6's body, with a phantom of CA-sar-TFMA imaged adjacent to the body. The center panel shows the ^{19}F MR image of the same cross-section. The right-most panel shows an overlay of the ^{1}H and ^{19}F images. CA-sar-TFMA signal intensity of the gallbladder region of interest (ROI) was normalized to the phantom ROI, and gallbladder concentration was calculated to be 34.2 mM.

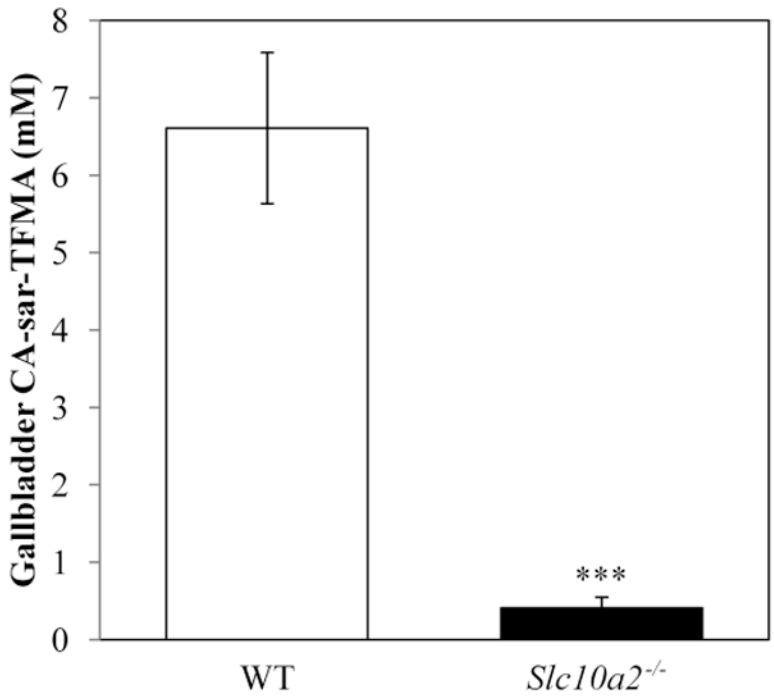

Figure 8.

Gallbladder concentration of CA-sar-TFMA in WT and knockout (*Slc10A2*$^{-/-}$) mice (n = 4 each). Mice were gavaged with 150 mg/kg CA-sar-TFMA and euthanized 7 h later. LC/MS/MS analysis showed a significant difference in gallbladder concentration between the two groups (6.61 ± 0.98 mM in WT mice vs. 0.41 ± 0.14 mM in knockout mice, p = 0.0008).

Table 1

in vivo Pilot Study Results 7 h after Oral Administration of 150 mg/kg CA-sar-TFMA

Mouse #	Gallbladder Weight (mg)	Gallbladder Conc. (mM)	Liver Conc. (μM)	Plasma Conc. (μM)
1	30	16.5	20.8	1.31
2	23	25.0	16.0	1.49
3	27	17.2	12.9	1.81
4	36	16.9	9.5	0.94
5	30	16.5	13.5	1.47

CA-sar-TFMA showed high accumulation in the mouse gallbladder and was present in much lower amounts in liver and plasma.